

# Origin of ferromagnetism in (Zn,Co)O from magnetization and spin-dependent magnetoresistance

T. Dietl,<sup>1,2,3</sup> T. Andrearczyk,<sup>1</sup> A. Lipińska,<sup>1</sup> M. Kiećana,<sup>1</sup> Maureen Tay,<sup>4,5</sup> and Yihong Wu<sup>4</sup>

<sup>1</sup>*Institute of Physics, Polish Academy of Science,  
al. Lotników 32/46, PL 02-668 Warszawa, Poland*

<sup>2</sup>*Institute of Theoretical Physics, Warsaw University, PL 00-681 Warszawa, Poland*

<sup>3</sup>*ERATO Semiconductor Spintronics Project, Japan Science and Technology Agency,  
al. Lotników 32/46, PL 02-668 Warszawa, Poland*

<sup>4</sup>*Department of Electrical and Computer Engineering,  
National University of Singapore, 4 Engineering Drive 3, Singapore 117576*

<sup>5</sup>*Data Storage Institute, 5 Engineering Drive 1, Singapore 117608*

(Dated: February 1, 2008)

In order to elucidate the nature of ferromagnetic signatures observed in (Zn,Co)O we have examined experimentally and theoretically magnetic properties and spin-dependent quantum localization effects that control low-temperature magnetoresistance. Our findings, together with a thorough structural characterization, substantiate the model assigning spontaneous magnetization of (Zn,Co)O to uncompensated spins at the surface of antiferromagnetic nanocrystal of Co-rich wurtzite (Zn,Co)O. The model explains a large anisotropy observed in both magnetization and magnetoresistance in terms of spin hamiltonian of Co ions in the crystal field of the wurtzite lattice.

PACS numbers: 75.50.Pp, 72.15.Rn, 72.25.Rb, 72.80.Ey

## I. INTRODUCTION

Since the discovery of ferromagnetic signatures in (Zn,Co)O,<sup>1</sup> this material has reached the status of a model system representing the ever increasing class of wide-band gap diluted magnetic semiconductors (DMS), diluted magnetic oxides (DMO), and non-magnetic oxides, in which challenging high-temperature ferromagnetism is observed under some growth conditions and/or post-growth processing.<sup>2,3,4,5</sup> In this paper, we present results of magnetization and magnetoresistance measurements of (Zn,Co)O:Al, whose quantitative interpretation substantiates the recent suggestion<sup>6,7</sup> that the puzzling ferromagnetic behavior can originate from uncompensated spins at the surface of wurtzite nanocrystals of Co-rich (Zn,Co)O. These nanocrystals are immersed in a Co-poor paramagnetic (Zn,Co)O matrix which, as we demonstrate here, determines magnetotransport properties of the system. Since the nanocrystals are coherent, *i. e.*, their crystallographic structure and lattice constant are identical to the surrounding (Zn,Co)O, they escape from the detection by standard HR XDR or TEM.

## II. SAMPLES AND EXPERIMENTAL SETUP

The studied (Zn,Co)O thin films are deposited by sputtering on (0001) sapphire ( $\alpha$ -Al<sub>2</sub>O<sub>3</sub>) substrates, so that the *c*-axis of the wurtzite structure is perpendicular to the film plane. A multi-chamber high vacuum system with a base pressure  $< 10^{-7}$  Torr is employed. Sintered ZnO, Al<sub>2</sub>O<sub>3</sub>, and Co targets are used as the sputtering sources for ZnO, Al, and Co, respectively. The samples are sputtered in an atmosphere of pure Ar gas at a pressure of 5 mTorr. Prior to deposition, the substrates are cleaned

using Ar reverse sputtering at 20 mTorr in a pre-cleaning chamber. A series of experiments has been carried out to optimize the substrate temperature and sputtering powers in order to obtain films with low resistivity. At a substrate temperature of 500°C, ZnO sputtering power of 150 W and Al<sub>2</sub>O<sub>3</sub> sputtering power of 30 W, the resistivity of as-grown ZnO:Al film was about  $10^{-3}$   $\Omega$ cm at room temperature. These conditions are employed to deposit Co-doped samples in which the Co composition *x* varied by changing the Co sputtering power from 3 to 50 W. The obtained x-ray diffraction patterns and the corresponding pole figure diagrams show that the films are well textured in the (0001) direction for *x* < 0.25.

We focus here on results obtained for non-magnetic ZnO:Al and for Zn<sub>0.95</sub>Co<sub>0.05</sub>O:Al showing clear ferromagnetic signatures. The Co content *x* is determined by x-ray photoelectron spectroscopy. The thickness for both films *d* = 200 nm has been confirmed by transmission electron microscopy (TEM). A careful examination by high resolution x-ray diffraction (HR XDR) and HR TEM demonstrates a good wurtzite structure of the films without evidences for precipitates of a secondary crystallographic phase, such as Co precipitates which are often present, especially in samples with high Co content.

We employ a high-field SQUID system for the magnetic studies. For electrical characterizations, Hall bars with a size  $324 \times 80$   $\mu$ m<sup>2</sup> are fabricated using a direct laser writer in a combination with ion milling. An Al/Au bilayer is deposited in order to obtain Ohmic contacts. All electrical measurements have been carried by a DC method with the current set as 100  $\mu$ A – a low limit ensuring an adequate signal-to-noise ratio in the employed setup. No indications of anomalous Hall effect have been detected. A uniform Al doping results in the high and almost temperature independent electron concentrations

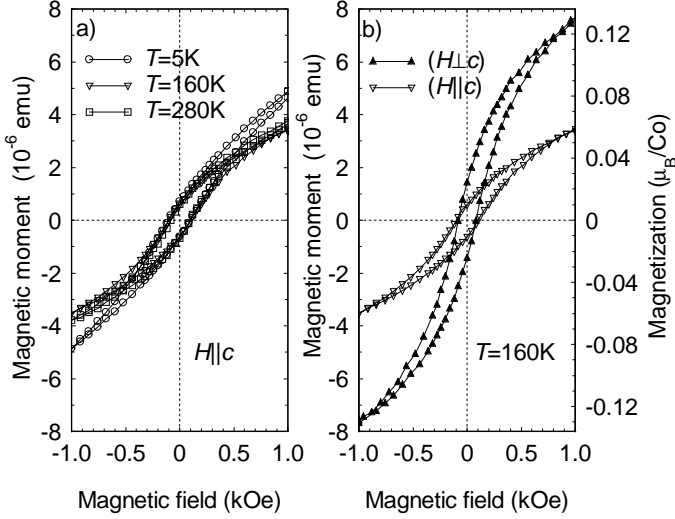


FIG. 1: Hysteresis loop of  $\text{Zn}_{0.95}\text{Co}_{0.05}\text{O:Al}$  measured as a function of external magnetic field; (a) for different temperatures and (b) for two directions of the magnetic field in respect to the wurtzite  $c$ -axis. A temperature independent contribution linear in the field is subtracted from the data.

$n = 1.7$  and  $1.1 \times 10^{20} \text{ cm}^{-3}$ , for  $x = 0$  and 5%, respectively, according to the Hall effect data. The presence of degenerate electrons with a band mobility value indicates that the Co acceptor state  $\text{Co}^{2+}/\text{Co}^{+1}$  is well above the bottom of the conduction band in ZnO.

### III. EXPERIMENTAL RESULTS

#### A. Magnetization measurements

Magnetization measurements of the  $\text{Zn}_{0.95}\text{Co}_{0.05}\text{O:Al}$  sample show well-developed hysteresis up to room temperature with a coercivity of about 50 Oe, as shown in Fig. 1. The presence of a robust ferromagnetism is indeed surprising since the *electron*-mediated spin-spin interaction is not expected to result in a ferromagnetic order above 1 K in DMS in question.<sup>8,9,10</sup> An important aspect of the results is a strong anisotropy: magnetization is significantly larger for the in-plane magnetic field. This indicates that shape magnetic anisotropy is overcompensated by crystalline magnetic anisotropy. The data point to the presence of the easy plane perpendicular to the  $c$ -axis of the wurtzite structure.

A comparison of magnetization data obtained after cooling without the magnetic field and with the magnetic field depicted in Fig. 2 shows a behavior indicative of superparamagnetism. According to these results, the blocking reaches the room temperature.

As shown in in Fig. 3, the hysteresis are superimposed on a background which is linear in the magnetic field with a slop increasing when temperature decreases. We evaluate that about 50% of Co ions contributes to this

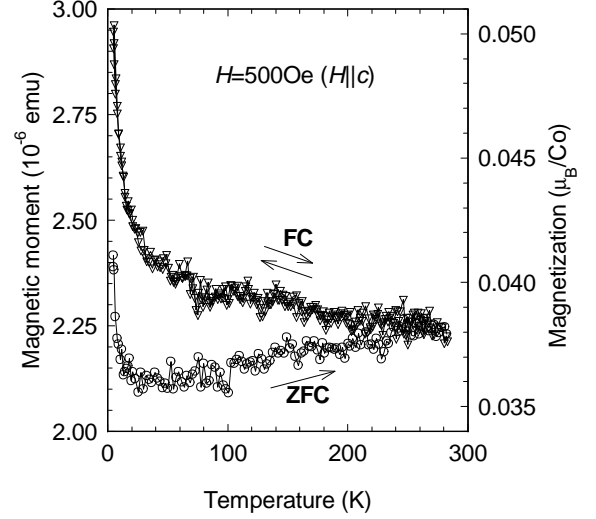


FIG. 2: Magnetization of  $\text{Zn}_{0.95}\text{Co}_{0.05}\text{O:Al}$  measured as a function of temperature, at magnetic field 500 Oe in  $H \parallel c$  configuration. The arrows indicate direction of temperature ramp. The zero field cooled (ZFC) and field cooled (FC) data were obtained after earlier cooling of the sample from 280 K down to 5 K without and with the applied magnetic field, respectively. A temperature independent contribution linear in the field is subtracted from the data.

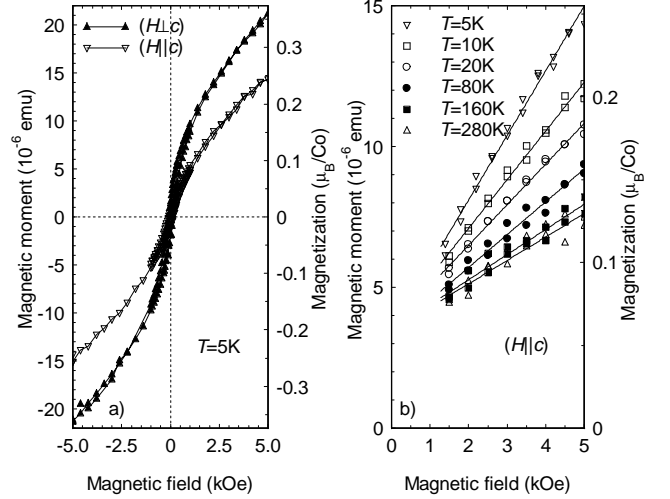


FIG. 3: Magnetization of  $\text{Zn}_{0.95}\text{Co}_{0.05}\text{O:Al}$  measured as a function of the external magnetic field; (a) for two directions of the magnetic field in respect to the wurtzite  $c$ -axis; (b) for different temperatures. The straight lines result from fitting to the data in a high field range. A temperature independent contribution linear in the field is subtracted from the data.

paramagnetic response.

#### B. Magnetoresistance: non-magnetic $n$ -ZnO:Al

Figure 4(a) shows magnetoresistance (MR) of ZnO:Al in the magnetic field  $H$  applied parallel to the  $c$  axis. We

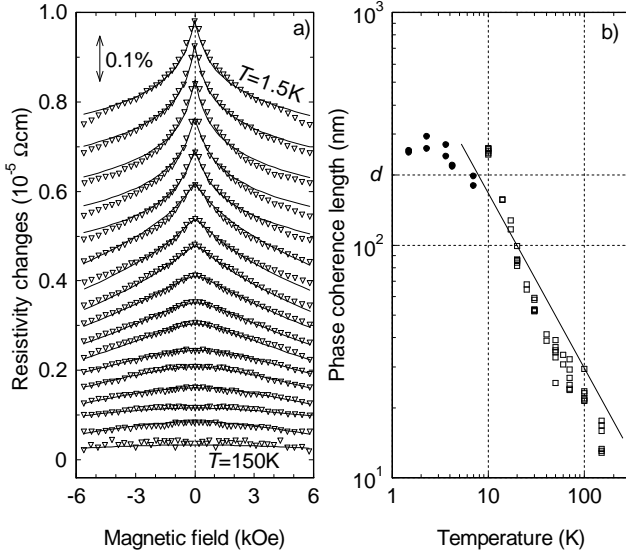


FIG. 4: (a) Resistivity changes in the magnetic field ( $H \parallel c$ ) for ZnO:Al (points) measured at  $T = 1.5, 2.3, 3.6, 4.2, 7, 10, 14, 17, 20, 25, 30, 40, 50, 60, 70, 100$  and  $150$  K. Curves are vertically shifted for clarity. The fitted curves (lines) are obtained within the weak localization (WL) theory. (b) Phase coherence length  $L_\varphi$  (which is the fitting parameter) as a function of temperature. The dots denote  $L_\varphi$  values determined by fitting 2D WL theory<sup>11,12,13</sup> and the squares by 3D one ( $L_\varphi < d$ ).<sup>11,13</sup> Straight line shows the  $T^{-3/4}$  dependence expected for 3D disordered systems.

have checked and confirmed that the shape of MR curve is independent of the applied field direction. As seen, MR is negative and becomes stronger with decreasing temperature. Such a character and magnitude of MR (of the order of 0.1% at  $T = 1.5$  K and  $H = 5$  kOe) are similar to those observed previously for ZnO:Al films grown by pulsed laser deposition technique<sup>14</sup> and for an accumulation layer on ZnO.<sup>15</sup> We anticipate, therefore, that similarly to those cases, MR results from quantum corrections to conductivity of disordered systems, that is from a destructive effect of the magnetic field (vector potential) on constructive interference corresponding to two time-reversal paths along the same self-crossing trajectories. The influence of this effect on MR can be quantitatively described in the weakly localized regime  $k_F l \gg 1$ , where  $k_F$  is the Fermi wave vector and  $l$  is the mean free path.<sup>13</sup> The value  $k_F l = 7$  is determined for our ZnO:Al sample.

In order to evaluate MR theoretically, we follow the procedure employed previously,<sup>14</sup> treating the phase coherence length  $L_\varphi$  as the only fitting parameter to independently determined MR curves at particular temperatures. The determined values of  $L_\varphi$  are employed in the MR simulations for (Zn,Co)O described below. The magnitude of  $L_\varphi$  and its temperature dependence  $L_\varphi \sim T^{-3/4}$  are similar to those found previously,<sup>14</sup> though  $L_\varphi(T)$  determined here starts to saturate at higher temperature. We associate this difference to electron heating

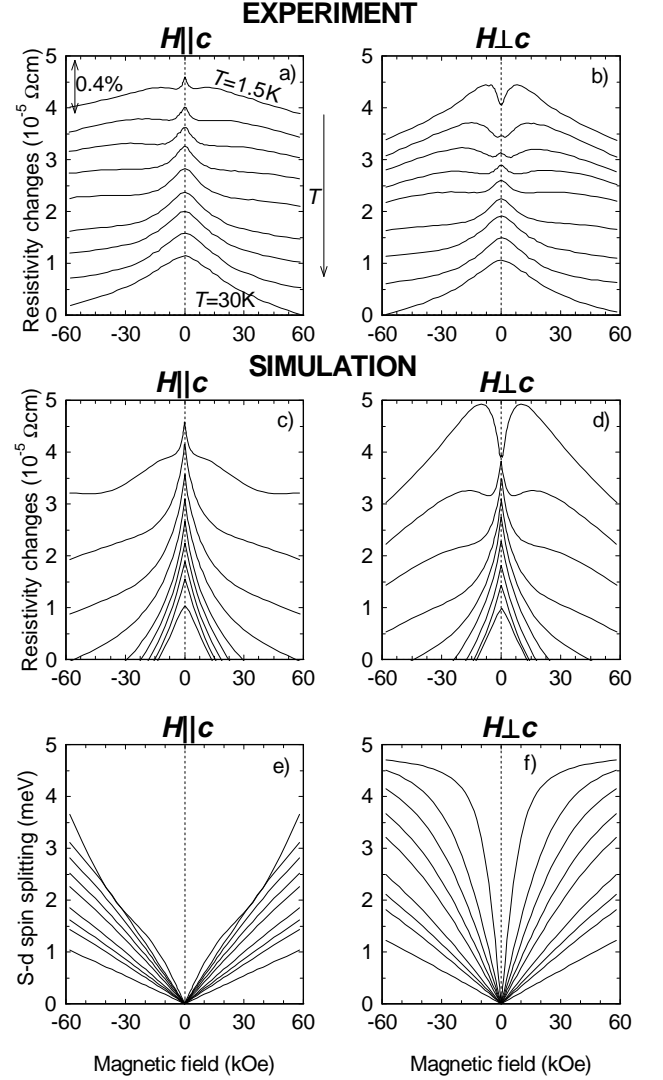


FIG. 5: Resistivity changes of  $\text{Zn}_{0.95}\text{Co}_{0.05}\text{O:Al}$  in the magnetic field, measured (a,b) and simulated (c,d) for temperatures  $T = 1.5, 4.2, 6, 8, 10, 14, 17, 20$  and  $30$  K. Curves are vertically shifted for clarity. Simulation of magnetic field dependence of Co-related spin-splitting (e,f) are performed for the same set of temperatures. The configuration of the external magnetic field is  $H \parallel c$  for (a,c,e) and  $H \perp c$  for (b,d,f).

by a relatively high current applied in the present setup.

### C. Magnetoresistance: magnetic $n\text{-Zn}_{0.95}\text{Co}_{0.05}\text{O:Al}$

The resistivity changes in the magnetic field as found for  $\text{Zn}_{0.95}\text{Co}_{0.05}\text{O:Al}$  are shown in Figs. 5(a) and 5(b) for  $H \parallel c$  and  $H \perp c$ , respectively. A positive MR component, absent in  $n\text{-ZnO}$ , is seen to take over with lowering temperature. A similar behavior, *i. e.*, the appearance of temperature-dependent *positive* MR in the presence of magnetic ions, has been previously observed for

$n$ -(Cd,Mn)Se,<sup>16</sup>  $n$ -(Cd,Mn)Te,<sup>17,18</sup>  $n$ -(Cd,Zn,Mn)Se,<sup>19</sup>, and  $n$ -(Zn,Mn)O.<sup>14</sup> Remarkably, however, no spontaneous magnetization was revealed in those materials, and positive MR was quantitatively described<sup>14,16,17,18,19</sup> by the effect of the field-induced giant spin-splitting on disorder-modified electron-electron interactions.<sup>13</sup> In accord with such an interpretation, no corresponding MR was found in ferromagnetic (Ga,Mn)As,<sup>20</sup> where hole states are spin-polarized already in the absence of an external magnetic field. On the other hand, contrary to the previous studies of paramagnetic wurtzite (wz) DMS,<sup>14,16</sup> MR of (Zn,Co)O reveals a dependence on the direction of the magnetic field in respect to the  $c$ -axis. As visible in Fig. 5, the positive component is stronger for the  $H \perp c$  case. We have checked that this MR does not depend on the orientation of the magnetic field in respect to the current direction. A sensible model of (Zn,Co)O has to elucidate, therefore, why *no* ferromagnetic signatures are observed in electron transport as well as explain large anisotropy of MR.

#### IV. DISCUSSION

We will now demonstrate that our findings, together with a number of puzzling data accumulated over the recent years,<sup>2,3,4,5,21,22</sup> can readily be interpreted in terms of nano-scale spinodal decomposition into antiferromagnetic Co-rich wz-(Zn,Co)O nanocrystals and a matrix of wz-(Zn,Co)O accounting for the paramagnetic contribution. According to this model, the ferromagnetic signatures result from uncompensated spins at the nanocrystal surface<sup>7</sup> and will be visible below both the Néel temperature  $T_N$  and the blocking temperature  $T_B$  of the nanocrystals. Such an effect has actually been visible in the case of NiO nanoparticles<sup>23</sup> and analyzed theoretically.<sup>24</sup>

The quantitative examination of magnetic susceptibility as a function of  $x$  in paramagnetic wz- $\text{Zn}_{1-x}\text{Co}_x\text{O}$  led to the extrapolated antiferromagnetic Curie-Weiss temperature as high as  $|\Theta| = 950 \pm 100$  K for  $x = 1$ ,<sup>3</sup> indicating that, indeed,  $T_N$  of the Co-rich wz-(Zn,Co)O can well surpass the room temperature. Furthermore, a non-zero value of the orbital momentum in the case of the  $S = 3/2$  spins of  $\text{Co}^{2+}$  ions in ZnO results in a relatively large magnitude of the single-ion magnetic uniaxial anisotropy energy  $D = 3.97$  K with the easy plane perpendicular to the  $c$ -axis.<sup>22</sup> Assuming that the in-plane anisotropy is 10 times smaller, the nanocrystals with the radius  $r = 3.7$  nm will exhibit  $T_B \approx 4\pi N_0 r^3 D S^2 / (30 \times 25)$  as high as 300 K, where  $N_0 = 4.2 \times 10^{22} \text{ cm}^{-3}$  is the cation concentration in ZnO.

Figure 6 shows spontaneous magnetization computed according to the above model for various nanocrystal shapes and dimensions. We have investigated type II and type III antiferromagnetic (AF) spin arrangement in the wurtzite structure.<sup>25</sup> A spherical nanocrystal of radius  $r$  is defined by fixing the origin at a certain lattice site

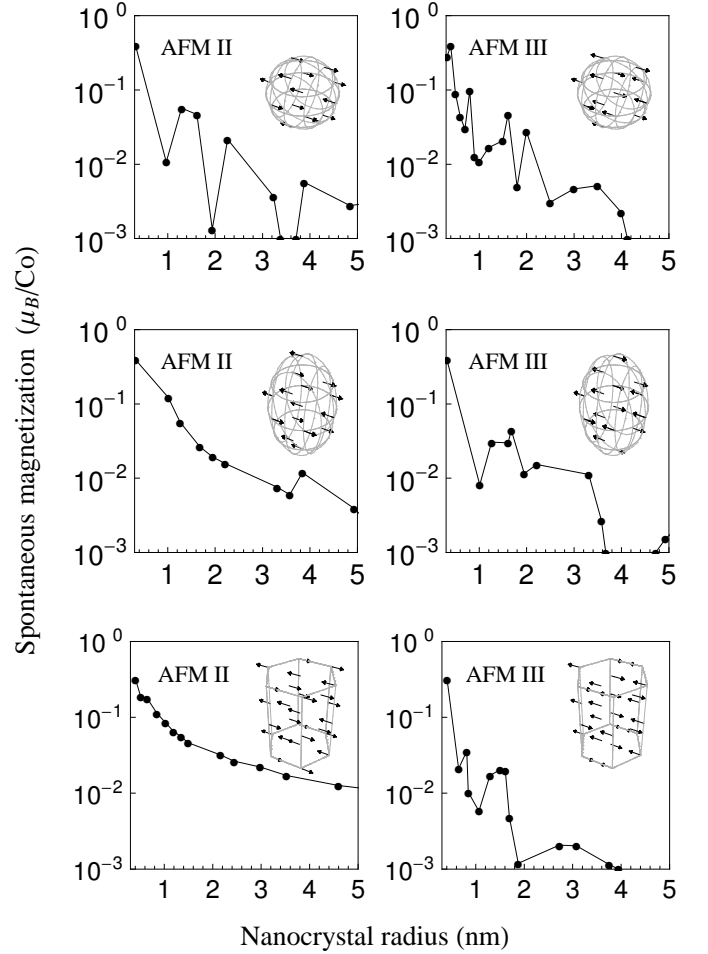


FIG. 6: Saturation magnetization of uncompensated Co-spins at the surfaces of antiferromagnetic wurtzite CoO nanocrystals, calculated as a function of the nanocrystal size for different nanocrystal shapes as indicated in the legend. It is assumed that a half (2.5%) of Co atoms in  $\text{Zn}_{0.95}\text{Co}_{0.05}\text{O}$  forms identical nanocrystals exhibiting type II or III antiferromagnetic ordering. The quoted radii correspond to spheres of the same volume. The magnetization value is given in the Bohr magnetons per one cobalt ion in  $\text{Zn}_{0.95}\text{Co}_{0.05}\text{O}$ .

and including all spins within the distance  $r$ .<sup>26</sup> The ellipsoid and hexagonal nanocrystals have been constructed in a similar way, defining  $r$  as the radius of a sphere of the same volume as the ellipsoid and hexagonal prism, respectively. We see that for the wurtzite prism and ellipsoid AFM II nanocrystals spontaneous magnetization attains significant values. In particular, for  $r = 3.7$  nm, as quoted above, spontaneous magnetization per Co ion reaches a few percent of the Bohr magneton, in agreement with the experimental results displayed in Figs. 1–3.

The presence of antiferromagnetic wz nanocrystals invoked here has important consequences for the interpretation of magnetization in thin (Zn,Co)O films. In particular, the term linear in the magnetic field, so far assumed to result from substrate diamagnetism and the

film paramagnetism, can actually contain a sizable contribution from the antiferromagnetic portion of the film. Furthermore, Co-precipitates are known to act as nucleation centers for CoO, which exert an exchange bias on the Co cores.<sup>27</sup> Accordingly, the ferromagnetic-like response may originate, in general, from uncompensated spins at the nanocrystal surface but also from Co precipitates exchange biased by the surrounding Co-rich (Zn,Co)O. In either case, the large magnitude of uniaxial crystal-field anisotropy of Co in ZnO, corresponding to the anisotropy field  $H_A = 53$  kOe,<sup>22</sup> elucidates why the magnetic response observed by us (Figs. 1 and 3) and others<sup>4</sup> is much stronger for the  $H \perp c$  configuration comparing to the  $H \parallel c$  case. At the same time, it rules out precipitates of free standing metallic Co precipitates as the dominant source of ferromagnetic-like response in these samples. Importantly, this view is supported by x-ray absorption, x-ray magnetic circular dichroism (XMCD), and photoemission experiments for ferromagnetic (Zn,Co)O,<sup>21</sup> which demonstrate that Co atoms substitute Zn, assume the high spin 2+ charge state, and interact antiferromagnetically. Furthermore, within this scenario, the dependence of ferromagnetic response on growth conditions and processing<sup>4,5</sup> results from a sensitivity of the nanocrystal aggregation process to the co-doping.<sup>6,28</sup> The (Zn,Co)O nanocrystals in question can be, presumably, classified as Mott-Hubbard antiferromagnets. The corresponding insulating character together with a small magnitude of nanocrystal magnetization, account for weak ferromagnetic signatures in MCD spectra near the band gap of the host.<sup>5,29</sup> In the same way we explain the established here lack of ferromagnetic signatures in electron transport.

Taking the above arguments into account we assume that MR is determined by the properties of the paramagnetic (Zn,Co)O matrix. Owing to a large value of the relevant parameter  $k_{FL} \approx 3$  we can safely apply the previously developed approach<sup>14,16</sup> to the weak localization theory with the effects of electron-electron interactions taken into account.<sup>13</sup> We compute MR values employing the 3D formulae, as the diffusion constant is smaller in (Zn,Co)O comparing to ZnO, so that the dimensional cross-over occurs at lower temperature. There are two parameters describing the effect: the magnitude of the interaction in the triplet channel taken as<sup>13,16</sup>  $F_\sigma \equiv 2g_3 = 1$  and the spin-splitting of the conduction band. The splitting contains the Zeeman term  $g^*\mu_B B$ , with  $g^* = 2.0$ , and the s-d contribution,  $-x_{\text{eff}}\alpha N_0 \langle S_z \rangle$ . The exchange energy  $\alpha N_0 = 0.18$  eV is assumed, which was determined for wz-(Cd,Co)S,<sup>30</sup> a value close to those of Mn-based DMS.<sup>31</sup> Similar magnitudes of  $\alpha N_0$  in (II,Co)VI and (II,Mn)VI compounds is

consistent with the virtually identical values of the the s-d exchange energy for the free  $\text{Co}^{+1}$  and  $\text{Mn}^{+1}$  ions,  $J_{s-d} = 0.40$  eV.<sup>32</sup> The temperature and field dependent mean spin value along the field direction  $\langle S_z \rangle$  is numerically calculated from the spin hamiltonian of  $\text{Co}^{2+}$  ions in ZnO.<sup>22</sup> We assume here that a half of Co ions is randomly distributed over the paramagnetic host, which leads to  $x_{\text{eff}} = 0.018$  for  $x = 0.025$ .<sup>31</sup>

Figures 5(c,d) show the computed values of MR. In view that no adjustable parameters are involved, the agreement between experimental [Figs. 5(a,b)] and theoretical [Figs. 5(c,d)] findings is to be regarded as quite good. In particular, the theory reproduces MR shape and temperature dependence. Furthermore, clearly visible MR differences for the two configurations,  $H \parallel c$  and  $H \perp c$ , are well reproduced by the theory.

## V. CONCLUSIONS

The findings presented in this paper together with the results accumulated over recent years for (Zn,Co)O can consistently be interpreted in terms of spinodal decomposition into Co-rich antiferromagnetic nanocrystals embedded in the Co-poor (Zn,Co)O host. Within this scenario, presumably relevant to a number of other DMS and DMO, ferromagnetic signatures in the absence of ferromagnetic precipitates such as free standing Co clusters, result from uncompensated spins at the surface of the antiferromagnetic nanocrystals. The nanocrystal aggregation can be steered by growth conditions and co-doping,<sup>6,28</sup> as the position of the Fermi level affects the charge state and/or and the diffusion coefficient of transition metals in semiconductors. This explains the sensitivity of the ferromagnetic response to co-doping and deviations from stoichiometry found in (Zn,Co)O.<sup>2,4,5</sup> Importantly, this means that self-organized nano-assembling of magnetic nanocrystals in a semiconductor matrix can be controlled during the growth process.

## Acknowledgments

The work in Warsaw was supported in part by ER-ATO Semiconductor Spintronics Project of Japan Science and Technology Agency and by SPINTRA Project of European Science Foundation. The work at the National University of Singapore was supported by the A\*-STAR under Grant No. R-398-000-020-305. The authors are grateful to Zaibing Guo for the SQUID measurement.

<sup>1</sup> K. Ueda, H. Tabata, and T. Kawai, Appl. Phys. Lett. **79**, 988 (2001).

<sup>2</sup> K. Rode, A. Anane, R. Mattana, J.-P. Contour, O. Du-

rand, and R. LeBourgeois, J. Appl. Phys. **93**, 7676 (2003).  
<sup>3</sup> S. Kolesnik, B. Dabrowski, and J. Mais, J. Appl. Phys. **95**, 2582 (2004).

- <sup>4</sup> M. Venkatesan, C. B. Fitzgerald, J. G. Lunney, and J. M. D. Coey, Phys. Rev. Lett. **93**, 177206 (2004).
- <sup>5</sup> S. A. Chambers, T. C. Droubay, C. M. Wanga, K. M. Rosso, S. M. Heald, D. Schwartz, K. R. Kittilstved, and D. Gamelin, Materials Today **9**, 28 (2006), and references therein.
- <sup>6</sup> T. Dietl, Nature Mat. **5**, 673 (2006).
- <sup>7</sup> T. Dietl, Physica E **35**, 293 (2006).
- <sup>8</sup> T. Dietl, A. Haury, and Y. Merle d'Aubigné, Phys. Rev. B **B 55**, R3347 (1997).
- <sup>9</sup> T. Andrearczyk, J. Jaroszyński, M. Sawicki, Le Van Khoi, T. Dietl, D. Ferrand, C. Bourgognon, J. Cibert, S. Tatarenko, T. Fukumura, et al., in *Proceedings 25th International Conference on Physics of Semiconductors, Osaka, Japan, 2000*, edited by N. Miura and T. Ando (Springer, Berlin, 2001), p. 235.
- <sup>10</sup> N. A. Spaldin, Phys. Rev. B **69**, 125201 (2004).
- <sup>11</sup> B. L. Altshuler, A. G. Aronov, D. E. Khmel'nitskii, and A. I. Larkin, in *Quantum Theory of Solids*, edited by I. M. Lifshits (Mir, Moscow, 1982), p. 130.
- <sup>12</sup> A. Kawabata, J. Phys. Soc. Jpn. **49**, 628 (1980).
- <sup>13</sup> B. L. Altshuler and A. G. Aronov, in *Electron-Electron Interactions in Disordered Systems*, edited by A. L. Efros and M. Pollak (North Holland, Amsterdam, 1985), p. 1; H. Fukuyama, *ibid.*, p. 155; P. A. Lee and T. V. Ramakrishnan, Rev. Mod. Phys **57**, 287 (1985).
- <sup>14</sup> T. Andrearczyk, J. Jaroszyński, G. Grabecki, T. Dietl, T. Fukumura, and M. Kawasaki, Phys. Rev. B **72**, 121309(R) (2005).
- <sup>15</sup> A. Goldenblum, V. Bogatu, T. Stoica, Y. Goldstein, and A. Many, Phys. Rev. B **60**, 5832 (1999).
- <sup>16</sup> M. Sawicki, T. Dietl, J. Kossut, J. Igalson, T. Wojtowicz, and W. Plesiewicz, Phys. Rev. Lett. **56**, 508 (1986).
- <sup>17</sup> Y. Shapira, N. F. Oliveira Jr., P. Becla, and T. Q. Vu, Phys. Rev. B **41**, 5931 (1990).
- <sup>18</sup> J. Jaroszyński, T. Andrearczyk, G. Karczewski, J. Wróbel, T. Wojtowicz, D. Popović, and T. Dietl, Phys. Rev. B **76**, 045322 (2007).
- <sup>19</sup> I. P. Smorchkova, N. Samarth, J. M. Kikkawa, and D. D. Awschalom, Phys. Rev. Lett. **78**, 3571 (1997).
- <sup>20</sup> F. Matsukura, M. Sawicki, T. Dietl, D. Chiba, and H. Ohno, Physica E **21**, 1032 (2004).
- <sup>21</sup> M. Kobayashi, Y. Ishida, J. I. Hwang, T. Mizokawa, A. Fujimori, K. Mamiya, J. Okamoto, Y. Takeda, T. Okane, Y. Saitoh, et al., Phys. Rev. B **72**, 201201(R) (2005).
- <sup>22</sup> P. Sati, R. Hayn, R. Kuzian, S. Régnier, S. Schafer, A. Stepanov, C. Morhain, C. Deparis, M. Laugt, M. Goiran, et al., Phys. Rev. Lett. **96**, 017203 (2006).
- <sup>23</sup> E. Winkler, R. D. Zysler, J. I. Vasquez Mansilla, and T. Fiorani, **72**, 132409 (2005).
- <sup>24</sup> E. Eftaxias and K. N. Trohidou Phys. Rev. B **71**, 134406 (2005).
- <sup>25</sup> R. I. Hines, N. L. Allan, G. S. Bell and W. C. Mackrodt J. Phys.: Condens. Matter **9**, 7105 (1997).
- <sup>26</sup> K. N. Trohidou and J. A. Blackman Phys. Rev. B **41**, 9345 (1990).
- <sup>27</sup> J. B. Tracy, D. N. Weiss, D. P. Dinega, and M. G. Bawendi, Phys. Rev. B **72**, 064404 (2005).
- <sup>28</sup> S. Kuroda, N. Nishizawa, K. Takita, M. Mitome, Y. Bando, K. Osuch, and T. Dietl, Nature Mat. **6**, 440 (2007).
- <sup>29</sup> K. Ando, Science **312**, 1883 (2006).
- <sup>30</sup> U. Gennser, X. C. Liu, T. Q. Vu, D. Heiman, T. Fries, Y. Shapira, M. Demianiuk, and A. Twardowski, Phys. Rev. B **51**, 9606 (1995).
- <sup>31</sup> T. Dietl, in *Handbook of Semiconductors*, edited by T. S. Moss (North Holland, Amsterdam, 1994), vol. 3B, p. 1251.
- <sup>32</sup> A. Eucken, ed., *Landolt-Bornstein Encyclopedia* (Springer-Verlag, Berlin, 1950), vol. 1, p. 193.